Kinetics towards mechanism and real operation for ultra-deep hydrodesulfurization and hydrodenitrogenation of diesel

Yachen Yin[a], Wenbin Chen[b] , Guilian Wu[a], Feng Xin[a,*], Kang Qin[b], Yutao Lu[b], Le Zhang[b], Mingfeng Li[b,*]

[a] School of chemical engineering and technology, Tianjin University, Tianjin 300072, China

[b] Research Institute of Petroleum Processing, SINOPEC, 18 Xue Yuan Road, 100083 Beijing, People's Republic of China

[*]Corresponding Author: [a]E-mail: xinf@tju.edu.cn, Tel: +86-22-27409533, Fax: +86-22-27892359 [b]E-mail:limf.ripp@sinopec.com, Tel: +86-10-82368662

1. Abstract

As the hydrodesulfurization (HDS) of diesel achieves ultra-deepness, our understanding of its kinetics is still far from in-depth. Therefore, herein, two lumped kinetic models for the ultra-deep hydrodesulfurization (UHDS) and hydrodenitrogenation (HDN) are established based on experiments under a wide range of operating conditions. Meanwhile, a four-lump kinetic model of the aromatic hydrosaturation (AHS) is erected. Our kinetic models disclose thermodynamic decisiveness in UHDS, which is unreachable beyond a temperature upper limit or a pressure lower limit. We also reveals the unexpected temperature dependence of nitrogen inhibition to HDS, for less than 300℃ the nitrogen inhibition becomes even more potent despite nitrogen removal by HDN reactions. Subsequently, the HDS kinetics of total sulfur are deciphered as multi stages exist in the whole reaction coordinate. Accordingly, a four-stage conceptual model involving mechanism and rate laws is proposed to offer a better understanding of nitrogen inhibition, thermodynamics and kinetics in UHDS.

Topical Heading and Key Words: ultra-deep hydrodesulfurization; diesel hydrotreating; kinetics; nitrogen inhibition; hydrodenitrogenation.

2. Introduction

Stringent constraints on diesel sulfur (<10ppm)[1] coupled with more refractory diesel feedstock, e.g. light catalytic cycle oil, in which carbazole and its alkyl derivatives dominate nitrogenous species[2], have brought new research emphasis on the kinetics of diesel ultra-deep hydrodesulfurization (UHDS). On the one hand, the competition between HDS and hydrodenitrogenation (HDN) becomes the most significant among compounds in diesel[3,4]. On the other hand, the substituted dibenzothiophenes turn into the predominant sulfurous compounds.

Under the forgoing emphasis, there are two extreme approaches to model HDS reactions. One is the traditional simple power law model of one lump, which is not detailed enough to accurately interpret reaction pathways of UHDS[5,6,7]. The other is the kinetic model based on a structural method[8], which could even offer details of molecules with relatively high accuracy guaranteed by essentially infinite lumps. But such a complex model overshoots the industrial problems in diesel hydrotreating since what really matters is whether total sulfur, rather than individual sulfur molecules, could be reduced below the constraint or not. As an intermediate, kinetic models of multi-lumps were proposed[9,10,11]. Despite their integration with the state-of-art sulfur characterization techniques, these models failed to consider the competition between simultaneous HDS and HDN, which would falsify the real kinetics[12].

As a new emphasis, the research on the HDN and its competition with HDS is lacking, especially for carbazoles[2,13,14]. While the reaction network for the HDN of carbazoles has long been established by Nagai et al.[15]in 1980, by now a corresponding kinetic model has not been reported, which is not commensurate with the predominance of carbazoles in refractory diesel. Similarly, though the nitrogen inhibition has been well-studied, most of them were conducted

in steady-state and with little removal of nitrogenous species[16,17]. Noticing this problem, Ho et al.[18] studied the nitrogen inhibition in simultaneous HDS and HDN, but they used the pure model compounds, which may be inapplicable to diesel hydrotreating under industrial conditions.

Apart from the issues above, the role of thermodynamic equilibria in UHDS have to be addressed as well due to the reversibility of the preferred hydrogenation pathways for HDS of refractory sulfurs. Some researchers[12,19] thought no thermodynamic limitation on overall HDS reactions based on theoretical analysis or experiments with model compounds. However, in UHDS, the kinetic control would transform to thermodynamic control. At this time the analysis on the chemical equilibria from experiments of real diesel is necessary.

The present research aims better understanding the thermodynamic, kinetic, and nitrogen inhibition in UHDS by developing two kinetic models based on the detailed analytic results of sulfurous and nitrogenous compounds in diesel. For HDN, a mechanistic kinetic model of two lumps is introduced and integrated with kinetic models of HDS to quantify the dynamic nitrogen inhibition effects. For HDS, the sulfurous compounds in diesel are classified into three lumps to replace our previous one-lump and two-region kinetics[20] for its discontinuity. Finally, a set of kinetic models for diesel hydrotreating, including UHDS, HDN and aromatic hydrosaturation (AHS), are developed by fully interpreting our hydrotreating experiments under a wide range of pressure, temperature, space time, and ratio of gas to oil in high-throughput reactors and thereby estimating the model parameters.

3. Experimental

3.1. Diesel

80% straight-run diesel and 20% light catalytic cycle oil were blended to obtain the feed oil,

whose properties are listed in Table 1.

Table 1. Properties of the diesel feedstock

Properties	Values
Density at 20℃ (kg/m^3)	858.8
Total nitrogen (ppm=mg/kg)	220
Composition of sulfurous compounds (ppm=mg/kg)	
Total sulfur	12000
Thiophenes, alkyl-BTs	5888
DBT, C_1-DBTs, C_2-DBTs	2304
4- or(and) 6-substituted DBTs, C_{3+}-DBTs	3808
Composition of diesel (wt%)	
Total aromatics	36.0
Mono-aromatics	16.4
Di-aromatics	17.4
Tri-aromatics	2.2
Paraffins (wt%)	43.2
Naphthenes (wt%)	20.8
Distillation curve (ASTM D-2887-04a)/℃	
Initial boiling point (IBP)	210
10%	255
30%	285
50%	299
70%	320
90%	355
Final boiling point (FBP)	383

3.2. Catalyst

A commercial NiMo/γ-Al_2O_3 catalyst prepared by Sinopec Research Institute of Petroleum Processing was used in our experiments. Its specific surface area, total volume and average

diameter of pores were 177m^2/g, 0.343cm^3/g, 7.74nm, respectively. This commercial catalyst pellets were ground and sieved to collect particle size range of 250-380μm for filling the high-throughput reactors.

3.3. High-throughput reactor system

As shown in Figure 1, our high-throughput reactor system consisted of three sections, i.e. feeding section, reactor section and sampling section. The reactor section contained several parallel trickle-bed reactors with an inner parameter of 2.0 mm and various catalyst bed heights. In each reactor the catalyst bed was sandwiched by two inert layers of SiC particles . The temperature and pressure inside each reactor were controlled precisely to approach the preset values. Flowrates of both diesel and hydrogen were stabilized by mass-flow controllers.

During our experiments, diesel was pumped and mixed with compressed pure hydrogen in the feeding section, then the gas-liquid mixture fed into parallel reactors to form trickle. Once leaving reactors, the outlet stream of each reactor ran into a gas-liquid separator. The gas effluent of all reactors was merged and vented through sodium hydroxide aqueous solution for neutralization. The liquid effluent was sampled for subsequent off-line analyses.

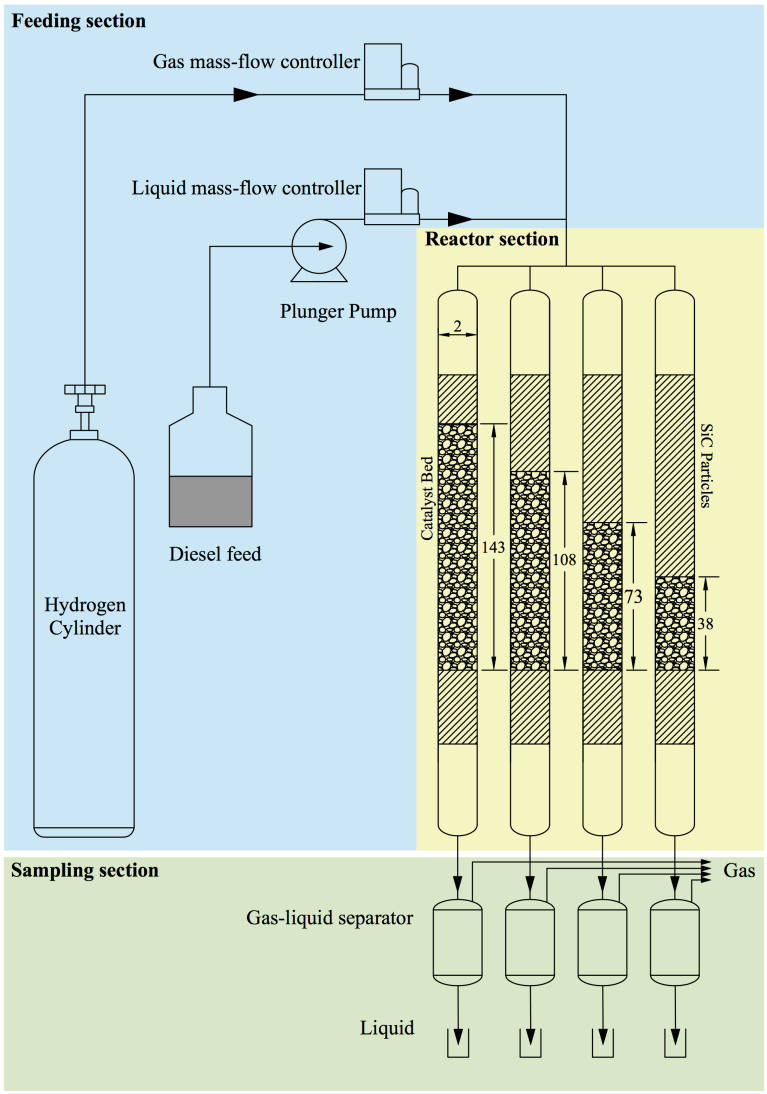

Figure 1. The schematic of an exemplar high-throughput reactor system

3.4. Experimental runs

With the forgoing setting, catalysts were loaded as example into four parallel trickle-bed reactors to reach the catalyst bed heights of 38 mm, 73 mm, 108 mm, and 143 mm, respectively. Prior to each run, the loaded catalysts were presulfurized under 6.4 MPa by vaporized kerosene solution containing 2% CS_2 at 250℃ for 6 hours and at 320℃ for 4 hours longer. Following the presulfurization, the catalysts were activated by hydrogenated diesel with 685 μg/g sulfur at 320℃. After 24 hours of activation, the diesel feedstock was switched to the kinetic experiments, where the time on stream of each experimental run was 72 hours.

In experiments, operating parameters, including temperature, pressure, gas-oil volumetric ratio $Q_{g,NTP}/Q_l$, liquid superficial velocity u_l, LHSV were varied within a wide range.

Details of experimental runs are listed in Table 2.

Table 2. Details of experimental runs

Run No.	T ℃	P MPa	$Q_{g,NTP}/Q_l$ m^3/m^3	τ hr
T-1	300			
T-2	320	6.4	300	0.18, 0.34, 0.50, 0.67
T-3	340			
T-4	360			
P-1		4.4		
P-2	340	5.4	300	0.18, 0.34, 0.50, 0.67
P-3		6.4		
P-4		7.4		
U-1				0.11, 0.20, 0.30, 0.40
U-2	340	6.4	300	0.18, 0.34, 0.50, 0.67
U-3				0.35, 0.68, 1.01, 1.33
Q-1			800	
Q-2	340	6.4	500	0.18, 0.34, 0.50, 0.67
Q-3			300	
Q-4			200	

3.5. Analytical techniques of samples

The sulfurous compounds in the diesel before and after hydrotreating were analyzed by Gas Chromatography-Sulfur Chemiluminescence Detection[21] (GC-SCD). Similarly, Gas Chromatography with Nitrogen chemiluminescence detector[22] (GC-NCD) was adopted to determine nitrogenous compounds. Composition of the diesel was determined by near-infrared spectroscopy method[23]. More details about the analytical techniques and their maximum errors could be found in supporting information.

4. Formulation of hydrotreating kinetic models

4.1. Vaporization of diesel

3 presents the mole fractions of vaporized feed f estimated by the Aspen Plus simulation software using equation of state of Redlich-Kong-Soaves[24] and flash module under our

experimental conditions. The values in Table 3 are almost identical to those in the experiments of vapor-liquid equilibrium[25]. Under typical conditions for UHDS, diesel vaporizes significantly even to 50 mol%, which would thin liquid film and concentrate the heavy species over the solid catalyst to affect the reaction rates[26,27].

Table 3. The mole fractions of vaporized diesel under experimental conditions

Run No.	f mol%	Run No.	f mol%	Run No.	f mol%
T-1	11.6	P-1	29.4	Q-1	50.0
T-2	16.0	P-2	25.2	Q-2	34.7
T-3	22.0	P-3	22.0	Q-3	22.0
T-4	30.1	P-4	19.6	Q-4	15.1

To quantify this effect, we correlate the apparent reaction rate constants of HDN and UHDS to the mole fractions of vaporized feed as expressed by Eq. (1) and (2).

$$k_{f,S_i} = (1 + f\alpha_{S_i})k_{l,S_i} \quad (1)$$

$$k_{f,N_i} = (1 + f\alpha_{N_i})k_{l,N_i} \quad (2)$$

where, α_{S_i} and α_{N_i} are named as vaporization factors to scale the effects of diesel vaporization to HDS and HDN reactions; k_{l,S_i} and k_{f,S_i} are the rate constants of UHDS at f = 0 or f, respectively; k_{l,N_i} and k_{f,N_i} are the rate constants of HDN at f = 0 or f, respectively.

As proved by Chen et al.[26], diesel vaporization can hardly affect AHS in diesel hydrotreating. So the effect of diesel vaporization is not considered in kinetic models of AHS.

4.2. The kinetic model of HDN

According to characterization results, carbazole and its derivatives dominate nitrogenous species in the diesel feed. So HDN reactions in this study are essentially equated with the nitrogen removals of carbazoles and its alkyl derivatives. For simplicity, carbazole and its alkyl

derivatives are grouped into one lump as N_1.

Similar to quinoline[28], HDN reactions of N_1 in this study appear to be non-first-order. Therefore, the HDN mechanism of carabazole over NiMo catalyst, rather than the simple power law, is referred for modelling as shown in Scheme 1[29]. It is noted that to trade off model details and experimental information[30], intermediates of hydrogenation pathway(Step 2-3 reactions in Scheme 1), i.e. partially hydrogenated carbazoles are lumped into another group as N_2.

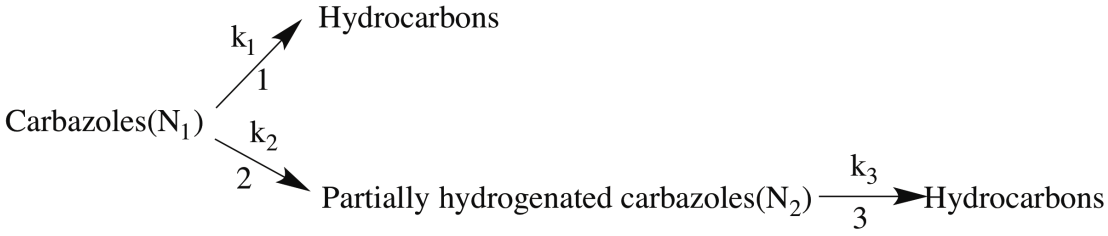

Scheme 1. The simplified scheme of hydrodenitrogenation of carbazole and its derivatives.

It is postulated that adsorption strength of N_1 on active sites for Step 1-3 reactions in Scheme 1 is predominant such that other adsorption terms like those of NH_3 and N_2 lump are negligible. In initial trials, it is found the non-zero adsorption constant of N_1 in direct HDN(Step 1 reaction in Scheme 1) can hardly fit the data. So it is further assumed the adsorption equilibrium constant of N_1 in direct HDN to be 0.

On the basis of above, for each step of reactions in Scheme 1, a Langmuir-Hinshelwood model is established as Eq. (3) to (5). It is noted that in Eq. (3) to (5), the effects of vaporization are included according to Eq. (2) with vaporization factors $\alpha_{N_1}, \alpha_{N_2}, \alpha_{N_3}$.

$$r_1 = k_{f,N_1} C_{N_1} P_{H_2}^{n_1} \tag{3}$$

$$r_2 = \frac{k_{f,N_2} C_{N_1} P_{H_2}^{n_2}}{\left(1 + K_1 C_{N_1}\right)^2} \tag{4}$$

$$r_3 = \frac{k_{f,N_3} C_{N_2} P_{H_2}^{n_3}}{\left(1 + K_2 C_{N_1}\right)^2} \tag{5}$$

where K_1, K_2 implies the reactions of hydrogenation and hydrogenolysis take place on two distinct active sites[31].

The squared denominator terms are also derived from initial trials, where the concentration profiles of N_1, N_2 produced by a power of 1 in the denominators can barely depict the nitrogen inhibition on UHDS. The rate constants and adsorption equilibrium constants are expressed by the Arrehenius equation and Van't Hoff equation, respectively.

Adding Eq.(3) and (5) yields the consumption rate of the total nitrogenous species:

$$r_N = k_{f,N_1} C_{N_1} P_{H_2}^{n_1} + \frac{k_{f,N_3} C_{N_2} P_{H_2}^{n_3}}{\left(1 + K_2 C_{N_1}\right)^2} \tag{6}$$

4.3. The kinetic model of HDS

As mentioned in the introduction, The simple power law model with one lump can hardly simulate the kinetics of UHDS accurately[5]. Herein, a three-lump kinetic model is designed. According to the rate constants offered by Ma et al.[32], the sulfurous compounds in the diesel feed are classified into three lumps named as S_1, S_2, and S_3, respectively. And the amount of each sulfurous lump is determined by characterization of samples from GC-SCD and lumped as presented in Figure 2.

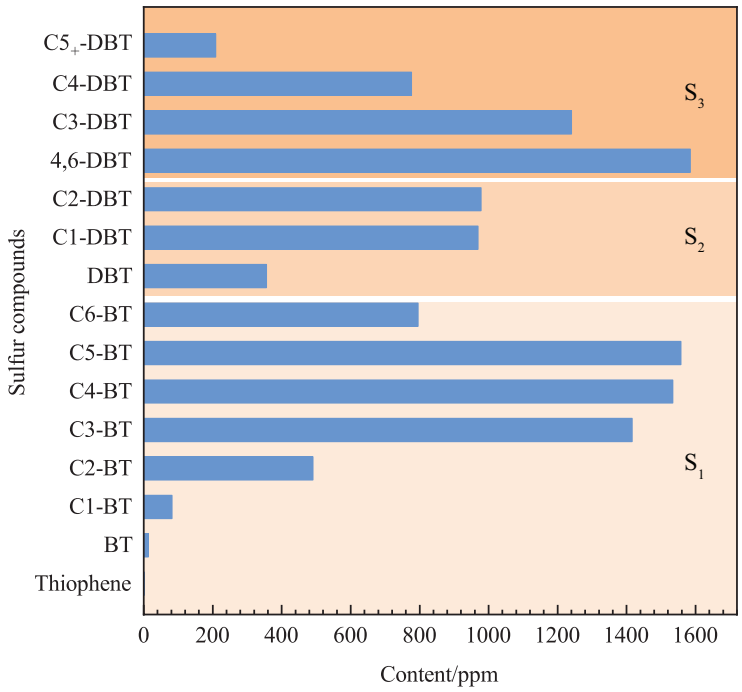

Figure 2.The distribution of sulfurous compounds in diesel feed(C1~C6-BT: benzothiophenes with 1 to 6 carbon substituents, C1~C4-DBT: dibenzothiophenes with 1 to 4 carbon substituents, $C5_+$-DBT: dibenzothiophenes with 5 or more carbon substituents, 4,6-DBT: dibenzothiophenes with alkyl substituents at 4- or(and) 6-position).

The lump S_1 consists of thiophene, benzothiophene (BT) and its alkyl substituted derivatives (C1~C6-BT). Ma et al[32] found that the individual sulfurous compounds in the same lump behave similar and follow the pseudo-first-order reaction. So the hydrodesulfurization rate of S_1 is

$$r_{S_1} = k_{f,S_1} C_{S_1} P_{H_2} \tag{7}$$

where the rate constant is modified according to Eq. (1) with α_{S_1}.

Dibenzothiophene (DBT) and dibenzothiophenes (C1~C2-DBT) with two alkyl substituents at neither 4- nor 6- position make up the lump S_2, where predominant HDS reaction pathway is the direct desulfurization, a pathway resistant to the nitrogen inhibition when the concentration of nitrogenous species is below 500ppm[33–35]. So similar to the lump S_1, UHDS of S_2 still

follows the first order rate equation, where the rate constant is modified by using Eq. (1) and α_{S_2} to get Eq. (8).

$$r_{S_2} = k_{f,S_2} C_{S_2} P_{H_2} \tag{8}$$

In a typical UHDS condition as 340℃, 6.4MPa, 300 m^3_{STP}/m^3, 1.5h^{-1}, the concentrations of lump S_1 and S_2 will be reduced to extremely low values, which enlarges the relative errors between simulations and sulfur characterization results. To reduce such errors, we sum up experiment data for the concentrations of S_1 and S_2 in each experimental run to produce new data and regress new data using Eq.(9).

$$r_{S_1+S_2} = k_{f,S_1} C_{S_1} P_{H_2} + k_{f,S_2} C_{S_2} P_{H_2} \tag{9}$$

Given their least reactivities, 4- or/and 6- substituted DBTs (4,6-DBT) and heavily substituted C3+-DBTs constitute the lump S_3[10]. As the most refractory sulfur lump, the predominant reaction pathway for HDS at low temperatures(e.g.<340℃) is hydrogenation (HYD) inhibited by the nitrogenous compounds dominantly[4,18]. However, the direct desulfurization (DDS), which is more resistant to nitrogenous compounds than HYD, becomes significant at high temperatures (e.g.>350℃)[36]. To describe such a dramatic shift in reaction pathway, a rate law with two terms denoting the DDS and HYD pathway is proposed. The reaction order for the DDS term(the first term on the left side of Eq.(10)) is assumed to be unity like HDS of S_1 and S_2. In the term for HYD pathway(the second term on the right side of Eq.(10)), a nitrogen inhibition denominator with n_6 as the fitting exponent is introduced according to the study of nitrogen inhibition effects[17] for this lump. The hydrogenation of refractory sulfurous compounds is a reversible reaction with an equilibrium concentration C_{S_e}(Eq.(11)), whose derivation shows in the appendix A. Finally, the rate equation is Eq. (10)

$$r_{S_3} = k_{f,S_3}\left(\mathrm{C}_{\mathrm{S}_3} - C_{S_e}\right) P_{H_2}^{n_4} + \frac{k'_{f,S_3}\left(\mathrm{C}_{\mathrm{S}_3} - C_{S_e}\right)}{\left(1 + K_{\mathrm{N1}} C_{N_1} + K_{\mathrm{N2}} C_{N_2}\right)^{n_6}} P_{H_2}^{n_5} \tag{10}$$

$$C_{S_e} = \frac{\left[C_{S_3}\right]_0}{1 + K_e \mathrm{C}_{\mathrm{H}_2}} \tag{11}$$

where n_4, n_5 are exponents of hydrogen and $n_4 = n_5 = 0.5$ according to our previous calculation[20].

Like other sulfurous compounds, we modify the rate constants in Eq. (10) using Eq. (1) and $\alpha_{S_3}, \alpha'_{S_3}$.

4.4. The kinetic model of AHS

The aromatics are classified into four lumps, namely mono-(A1), di-(A2), poly-(A3) aromatics, and non-aromatic compounds (A4) including both paraffinic and naphthenic compounds. The hydrogenations of different lumps take place as Scheme 2[24].

$$\text{polyaromatic(A3)} + \mathrm{H_2} \underset{\mathrm{k^r_{A3}}}{\overset{\mathrm{k_{A3}}}{\rightleftharpoons}} \text{diaromatic(A2)}$$

$$\text{diaromatic(A2)} + \mathrm{H_2} \underset{\mathrm{k^r_{A2}}}{\overset{\mathrm{k_{A2}}}{\rightleftharpoons}} \text{monoaromatic(A1)}$$

$$\text{monoaromatic(A1)} + \mathrm{H_2} \underset{\mathrm{k^r_{A1}}}{\overset{\mathrm{k_{A1}}}{\rightleftharpoons}} \text{Non-aromatics(A4)}$$

Scheme 2. The hydrogenation reactions of aromatics[24]

In Scheme 2 the forward reactions and the backward reactions are assigned as first order for the aromatics [24] to obtain the following rate equations Eq. (12) to (15):

$$r_{\mathrm{A3}} = k_{\mathrm{A3}}\, C_{\mathrm{A3}}\, P_{\mathrm{H_2}}^{n_7} - k^r_{\mathrm{A3}} C_{\mathrm{A2}} \tag{12}$$

$$r_{A2} = k_{\mathrm{A2}} C_{\mathrm{A2}} P_{\mathrm{H_2}}^{n_8} + k^r_{\mathrm{A3}} C_{\mathrm{A2}} - k^r_{A2} C_{\mathrm{A1}} - k_{\mathrm{A3}}\, C_{\mathrm{A3}}\, P_{\mathrm{H_2}}^{n_7} \tag{13}$$

$$r_{\mathrm{A1}} = k_{\mathrm{A1}} C_{\mathrm{A1}}\, P_{\mathrm{H_2}}^{n_9} + k^r_{A2} C_{A1} - k^r_{\mathrm{A1}} C_{\mathrm{A4}} - k_{\mathrm{A2}} C_{\mathrm{Di}} P_{\mathrm{H_2}}^{n_8} \tag{14}$$

$$r_{A4} = k^r_{\mathrm{A1}} C_{\mathrm{A4}} - k_{\mathrm{A1}} C_{\mathrm{A1}} P_{\mathrm{H_2}}^{n_9} \tag{15}$$

where n_7, n_8, n_9 are orders of hydrogen and $n_7 = n_8 = n_9 = 0.5$ from our previous calculation[20].

The temperature dependence of rate constants for the forward reactions and dehydrogenation of A4 in Eq. (12) to (15) are expressed by the Arrhenius equation.

5. The high-throughput reactor model

Since diameters of the reactors and the catalyst are so small, meanwhile velocities of the fluids in the bed are so high , we use the plug flow reactor model and assume: (1) the reactors are in isothermal operation; (2) diesel vaporizes only in the inert layer before the catalyst bed; (3) the hydrogen pressure and the gas velocity stay constant due to very excess hydrogen; (4) deactivation of catalyst is non-existent; (5) the catalyst is completely and uniformly wetted; Hereafter, an isothermal pseudo-homogeneous and one-dimensional reactor model for liquid phase is employed as Eq. (16a).

$$\frac{dC_i}{d\tau} = r_i \, , i = N, S_1 + S_2, S_3, A1, A2, A3, A4 \tag{16a}$$

The boundary conditions are:

$$\tau = 0: C_i = C_{i,0}, i = N, S_1 + S_2, S_3, A1, A2, A3, A4 \tag{16b}$$

where the molar concentrations of sulfurous compounds, nitrogenous species, and aromatics at reactor inlet are calculated using Eq.(16c).

$$C_{i,0} = \frac{\rho_l}{M_i} w_i, i = N, S_1 + S_2, S_3, A1, A2, A3, A4 \tag{16c}$$

w_i are the measured mass fractions of sulfurous, nitrogenous compounds and aromatics at reactor inlet. ρ_l is the measured density of diesel under experimental conditions. The relative molecular weight of S_1, S_2, S_3, and N are specified as that of their representatives, including benzothiophene, dibenzothiophene, dibenzothiophene, and carbazole, respectively. Meanwhile, the relative molecular weight of aromatics A1, A2, A3, A4, are set equal to that of benzene, naphthalene, anthracene, and diesel sample. The molecular weight of diesel sample is estimated by API methods[37].

6. Parameter estimation technique

To mitigate the negative effects of any potential outliers, the weighted least absolute error terms in Eq.(17) are set as the objective functions for parameter estimations of HDN, UHDS and AHS. The initial values of the rate constants and the activation energies are surmised from simple first order kinetic models, while the adsorption equilibrium constants and adsorption energies are initialized randomly.

$$SSE_i = \sum_{k=1}^{15} \sum_{j=1}^{4} w_i^{pj} \left| \left(C_i^{\mathrm{pj}}\right)_c - \left(C_i^{\mathrm{pj}}\right)_{exp} \right| \tag{17}$$

The interior point method is selected as the optimization method. Then, all parameters are estimated by self-coded MATLAB programs. The sequence for estimations is HDN before UHDS and AHS.

7. Results

7.1. Estimated parameters

The activation energies, pre-exponential factors and their 95% confidence intervals are summarized in Table 4. By parameter estimations, we discover that the parameters n_2 in Eq.(4) and $k_{\mathrm{A1}}^r, k_{\mathrm{A3}}^r$ in Eq.(12),(15) are statistically insignificant. Hence, the value of $n_2, k_{\mathrm{A1}}^r, k_{\mathrm{A3}}^r$ are specified as 0, which indicates the thermodynamic equilibria have no limitation on dehydrogenation reactions of A1 and A3 within 300-360℃.

Besides, in Table 4, all confidence intervals are narrow, which implies statistical significance of all parameters. Also the values of the energies of activation and adsorption are close to those in references used the similar feeds[6,7].

Table 4. Estimated parameters for hydrotreating reactions.

Reaction	Pre-exponential factor ln(A) $\ln(m^3/(mol\cdot MPa^{ni}))$	Activation energy E kJ/mol	Reaction order n
$S_1 \rightarrow HC^*$(Eq.(7))	$30.6 \pm 5.6 \times 10^{-3}$	$106.2 \pm 2.7 \times 10^{-2}$	1
$S_2 \rightarrow$HC(Eq.(8))	$28.5 \pm 8.0 \times 10^{-4}$	$106.9 \pm 3.9 \times 10^{-3}$	1
$S_3 \rightarrow$HC(HYD) (Eq.(10))	$9.5 \pm 1.5 \times 10^{-2}$	$10.3 \pm 7.7 \times 10^{-2}$	0.5
$S_3 \rightarrow$HC(DDS) (Eq.(10))	$84.8 \pm 3.6 \times 10^{-2}$	$407.5 \pm 1.7 \times 10^{-1}$	0.5
$N_1 \rightarrow$HC(Eq.(3))	$26.8 \pm 1.4 \times 10^{-2}$	$98.0 \pm 7.1 \times 10^{-2}$	$1.3 \pm 3.4 \times 10^{-3}$
$N_1 \rightarrow N_2$(Eq.(4))	$18.2 \pm 1.2 \times 10^{-1}$	$33.4 \pm 4.8 \times 10^{-1}$	$1.6 \pm 1.3 \times 10^{-3}$
$N_2 \rightarrow$HC(Eq.(5))	$33.8 \pm 1.4 \times 10^{-2}$	$130.8 \pm 5.8 \times 10^{-1}$	0
A3→A2(Eq.(12))	7.4 ± 4.7	52.4 ± 23.7	0.5
A2→A1(Eq.(13-14))	$15.3 \pm 1.7 \times 10^{-1}$	90.0 ± 0.9	0.5
A1→A2(Eq.(13-14))	$12.3 \pm 3.3 \times 10^{-1}$	82.8 ± 1.7	/
A1→A4(Eq.(15))	$13.9 \pm 2.3 \times 10^{-1}$	95.6 ± 1.2	0.5

*: HC denotes hydrocarbons.

The adsorption equilibrium constants listed in

Table 5 show all of the adsorptions being exothermic and having strong temperature dependence. By contrast, the temperature dependence of K_1(Eq.(4)) and K_{N1}(Eq.(10)) are found not statistically significant with the values of K_1 and K_{N1} being 52.8m^3/mol and 7.7 m^3/mol, respectively under experimental conditions. Such a great difference in the temperature dependence between adsorption of N_1 and N_2 on various active sites is probably caused by disparities in active sites and basicities of nitrogenous species.

Table 5. Estimated adsorption constants of N1 and N2.

Adsorption	Pre-exponential factor ln(B) ln(m^3/mol)	Adsorption enthalpy ΔH_{ads} kJ/mol
N_2 adsorption on active sites for S_3 hydrogenation(Eq.(10))	$81.3 \pm 5.6 \times 10^{-2}$	$-407.5 \pm 2.8 \times 10^{-2}$
N_1 adsorption on active sites for N_2 hydrogenolysis(Eq.(5))	$94.0 \pm 8.7 \times 10^{-1}$	-497.8 ± 4.0

As indicated by similar values of vaporization factors for HDS of S_2 and S_3, and hydrogenolysis of N_2 in Table 6, vaporization of diesel feed has almost the same impact on the rates of these reactions, which agrees with similar volatilities of S_2, S_3, and N_2 revealed by their close chemical structures and molecular weights. Meanwhile in initial trials, the values of the vaporization factor $\alpha_{S_1}, \alpha_{N_1}, \alpha_{N_2}$ approximate 0, which suggests vaporization effect is negligible to HDS of S_1 and HDN reactions involving N_1. So we set the value of $\alpha_{S_1}, \alpha_{N_1}, \alpha_{N_2}$ to be 0 directly in the following calculations.

Table 6. Estimated vaporization factors for HDS and HDN reactions.

Reaction	Vaporization factor $\alpha_{S_i}, \alpha_{N_i}$
$S_1 \rightarrow$ HC(Eq.(7))	0
$S_2 \rightarrow$ HC(Eq.(8))	$2.93 \pm 1.9 \times 10^{-4}$
$S_3 \rightarrow$ HC(HYD) (Eq.(10))	$2.97 \pm 2.06 \times 10^{-3}$
$S_3 \rightarrow$ HC(DDS) (Eq.(10))	$2.93 \pm 1.3 \times 10^{-2}$
$N_1 \rightarrow$ HC(Eq.(3))	0
$N_1 \rightarrow N_2$(Eq.(4))	0
$N_2 \rightarrow$ HC(Eq.(5))	$2.6 \pm 1.1 \times 10^{-1}$

7.2. Consistency in trends

Figure 3Figure 5 enumerates the calculated evolution of sulfurous, nitrogenous, aromatic compounds under all experimental conditions. The calculated results agree well with their experimental counterparts, which justifies our proposed models.

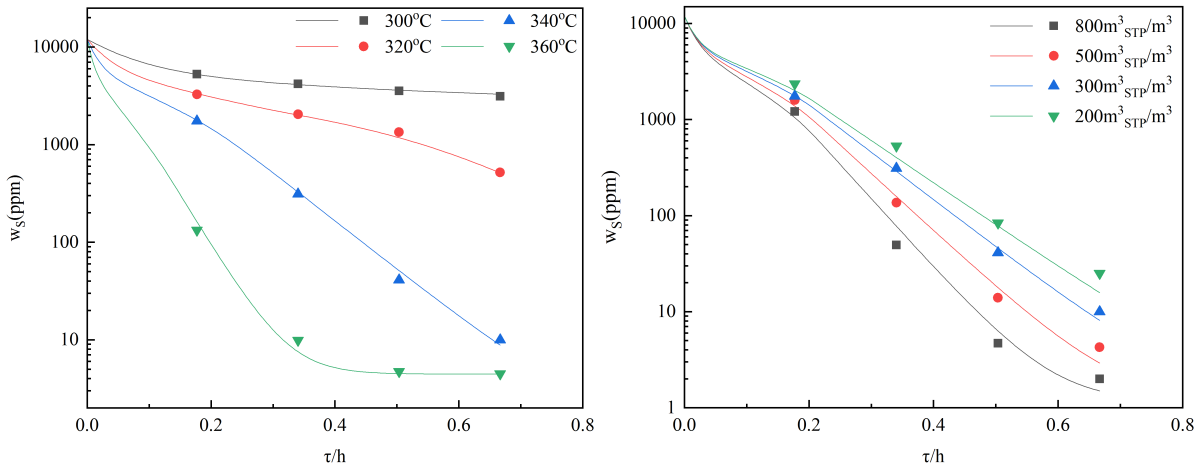

(a) (b)

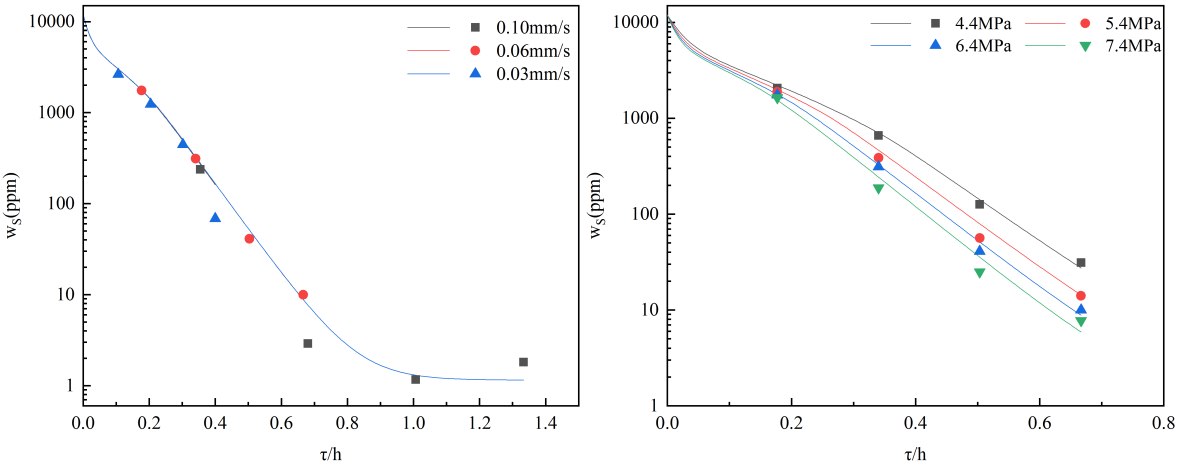

Figure 3.The simulated(lines) and experimental(points) concentration profiles of sulfurous compounds (a) under different temperatures(6.4MPa, 300 m^3_{STP}/m^3) (b) under different ratio of gas to oil (6.4MPa, 340℃) (c) under different superficial velocity(6.4MPa, 340℃) (d) under different pressures (300 m^3_{STP}/m^3, 340℃).

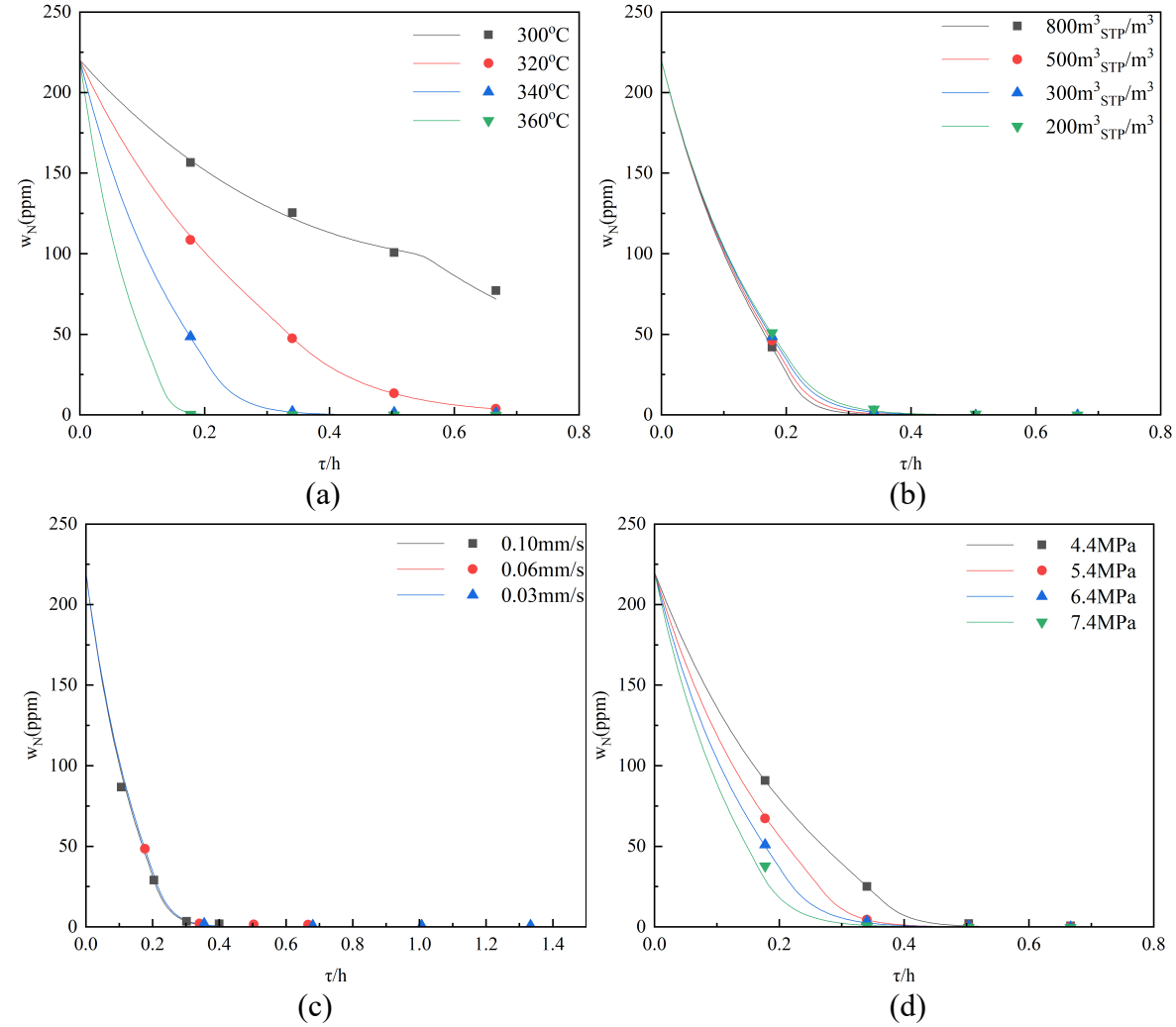

Figure 4.The simulated(lines) and experimental(points) concentration profiles of nitrogenous compounds (a) under different temperatures(6.4MPa, 300 m^3_{STP}/m^3) (b) under different ratio of gas to oil (6.4MPa, 340℃) (c) under different superficial velocity(6.4MPa, 340℃) (d) under different pressures (300 m^3_{STP}/m^3, 340℃).

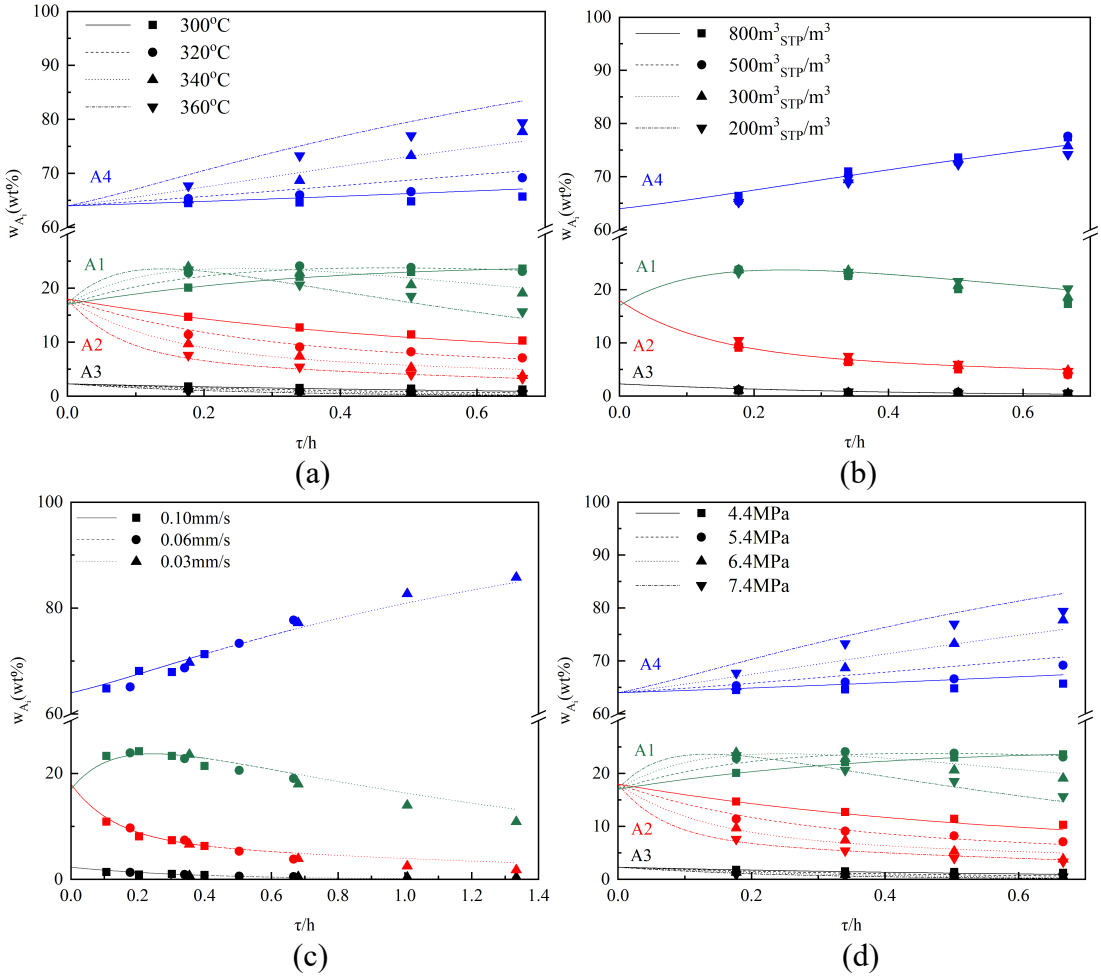

Figure 5.The simulated(lines) and experimental(points) concentration profiles of hydrocarbon compounds (a) under different temperatures(6.4MPa, 300 m^3_{STP}/m^3) (b) under different ratio of gas to oil(6.4MPa, 340℃) (c) under different superficial velocity(6.4MPa, 340℃) (d) under different pressures (300 m^3_{STP}/m^3, 340℃).

Using the estimated values of parameters in Table 4, we find the rate constant for HYD pathway in HDS of S_3 varies very little with temperatures, which is in stark contrast with the drastic change of DDS rate constant under different temperatures. This trend is consistent with HDS experiments of 4,6-DBT[1,36,38], which further corroborates our proposed models.

7.3. Comparison with experimental results

Figure 6 (a)-(b) compare the model results with their experimental counterparts. All simulated results of nitrogen, S_1, S_2, and A1~A4 deviate less than 10% from the experimental values. For S_3, the relative deviation from the experimental values is no more than 15% in non-ultra-deep regime (>100ppm). The little deviation and the Pearson coefficients close to 1 ensure the high accuracy of kinetic models. In ultra-deep regime (<10ppm), the magnified plot on the corner of Figure 6 (a) verifies that our model could predict whether the standard of sulfur in diesel (<10ppm) could be achieved or not under industrial conditions.

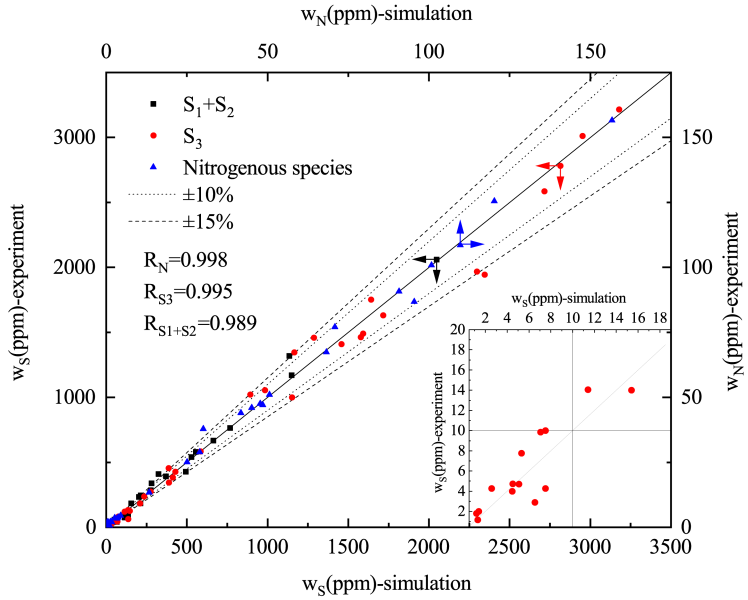

Figure 6. Comparison between experimental and simulated results (a) for HDS, HDN

kinetic models, and UHDS close to ultra-deepness(<10ppm) (b) for AHS kinetic models.

7.4. Sensitivity analyses of parameters

The sensitivity analyses of parameters for all kinetic models are summarized in Figure 7(a)-(d). All estimated parameters are indeed the optimum point since higher values of objective functions(the corresponding SSE in Eq.(17)) are presented by their neighboring points.

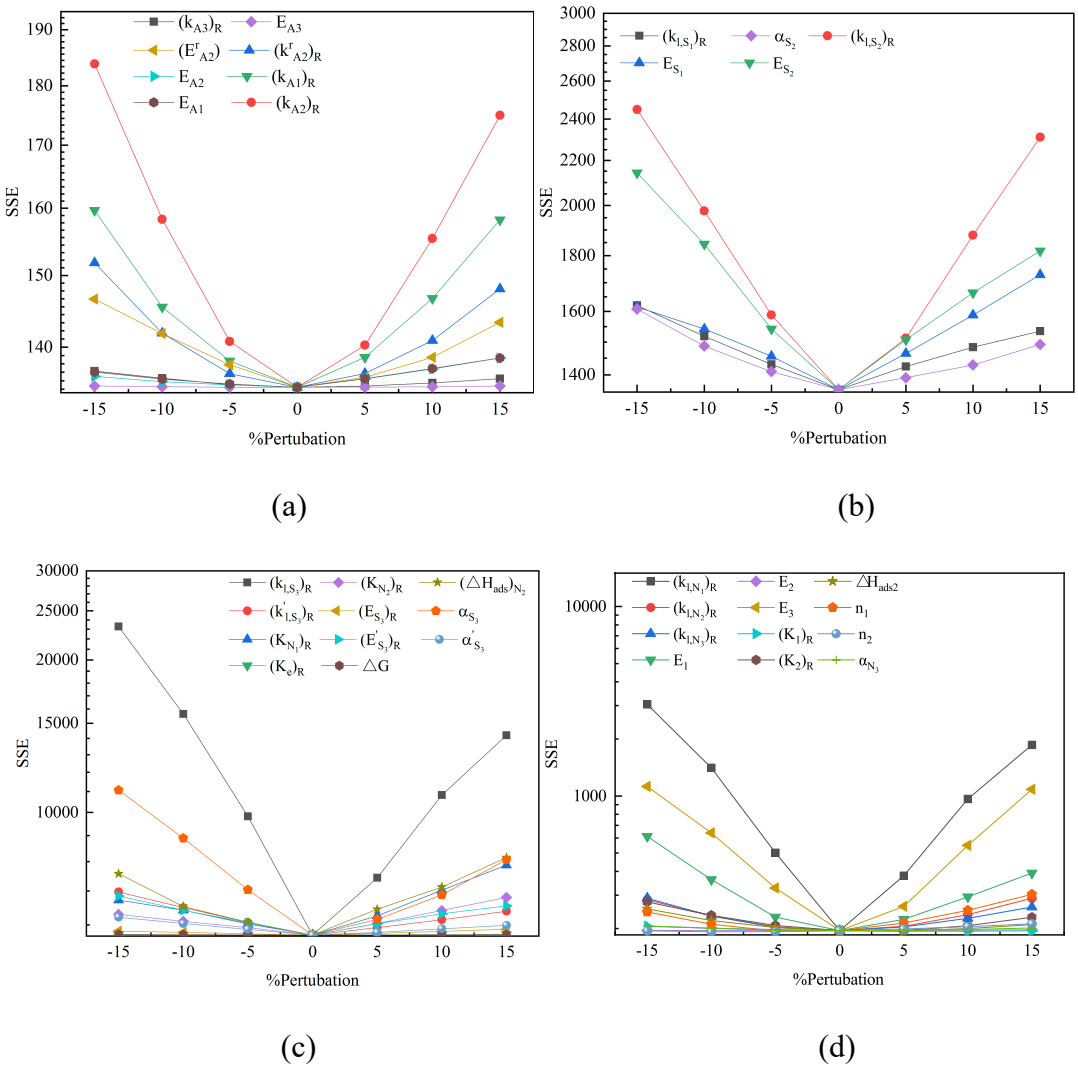

Figure 7.The sensitivity analysis of estimated parameters for (a) AHS; (b) UHDS of S_1 and S_2; (c) UHDS of S_3; (d) HDN.

8. Discussion

8.1. Thermodynamic limitation on UHDS

The thermodynamic equilibrium plays a role in our experimental and simulated results for the UHDS as shown in Figure 3(a) to Figure 3(d), where the concentration profiles of the lump S_3 suddenly hit a plateau when the UHDS achieves ultra-high conversion at higher temperature or lower space velocity in Figure 3(a) and Figure 3(c) respectively. Especially when temperature rises from 340℃ to 360℃, the lowest concentration representing the plateau raises too. This phenomenon agrees to the equilibrium law of exothermic reaction. Therefore, it is reasonable to believe that chemical equilibrium of the most refractory sulfurous compounds decides the inferior limit of sulfur removal. In order to unveil the decisiveness of the equilibrium quantitatively, we predict the equilibrium concentration in UHDS using Eq.(11) and plot Figure 8.

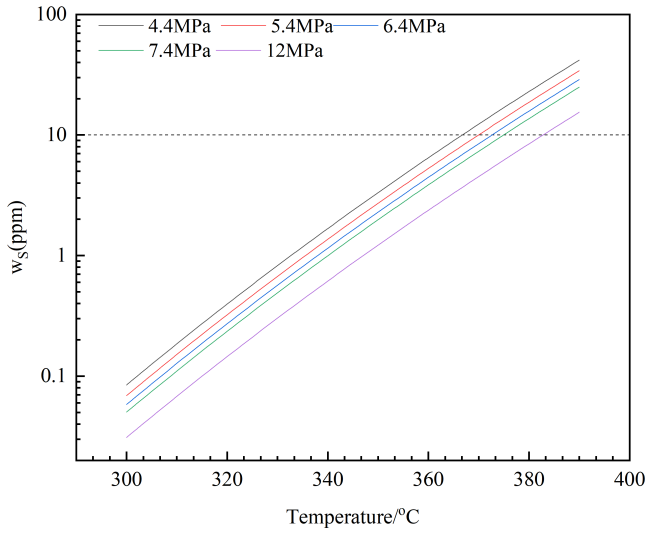

Figure 8. The predicted equilibrium concentration of S_3 vs. temperature under different pressures.

As shown in Figure 8, with the temperature increase, the equilibrium concentration of sulfurous compounds could exceed the constraint of 10ppm and thus the UHDS(<10ppm) becomes thermodynamically impossible. At a medium pressure of 6.4MPa and example temperature

375℃, the equilibrium concentration (i.e. the inferior limit of sulfur removal by HDS) is 10ppm, which means above 375℃, however long the space time is, the UHDS may not be achieved. While increase of pressure could reduce the equilibrium concentration but this effect decays as pressure is really low.

Besides the decisive role in the final result of UHDS, the discrepancy in activation energies for HYD and DDS, as shown in Table 4, reveals that the thermodynamic equilibrium also affect the selectivity of HDS for S_3. Due to the thermodynamic limitation in HYD pathway, the apparent activation energy of HYD pathway is significantly reduced[11]. Thus, HYD pathway contributes dominantly to HDS of S_3 at low temperatures(<340℃) while the DDS pathway becomes significant at reactor temperature above 360℃[36].

8.2. Dynamic nitrogen inhibition

As carbazole and its alkyl derivatives(N_1) are hydrogenated considerably under current conditions, the partially hydrogenated carbazole (N_2) as an intermediate exists in a large amount. Thus, both N_1 and N_2 lump compete with Sulfurous compounds for active sites and contribute to the nitrogen inhibition to HDS.

Compared with that of non-basic N_1 lump, the adsorption of basic N_2 lump on active sites for HDS has greater temperature dependence as shown by Rana et al.[39]. The adsorption equilibrium constants obtained by calculation from

Table 5 suggest the nitrogen inhibition to HDS is mainly from the π-mode adsorption of N_1 at temperature above 320℃. But as temperature drops, the main nitrogen inhibition shifts to the strong interaction with acidic active sites by N_2.

The calculated concentration profiles of N_1 and N_2 in Figure 9 show that the concentration of N_1 declines with rate increase caused by decaying self-inhibition, while concentration of the intermediate N_2 increases till a peak and contributes to HDN of nitrogenous species singlehandedly afterwards.

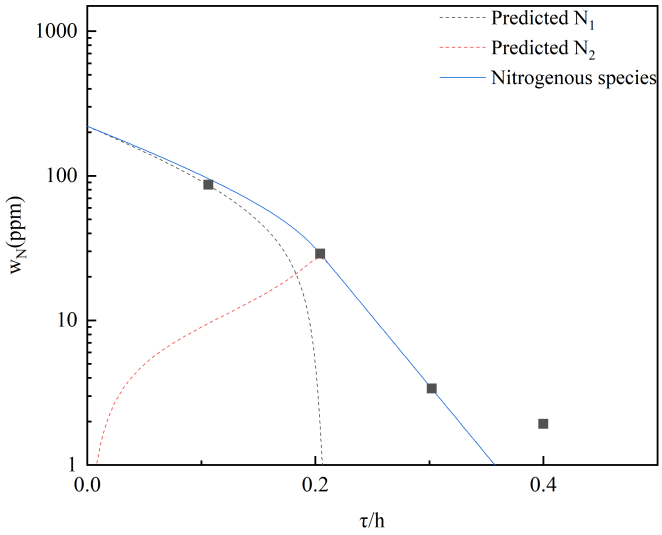

Figure 9.The concentration profiles of N_1, N_2, and total nitrogenous species(340°C, 6.4MPa, 300 m^3_{STP}/m^3).

$$r_{S_3} = k'\left(C_{S_3} - C_{S_e}\right)P_{H_2}^{0.5} \tag{18}$$

We reparameterize the HYD term in the rate equation Eq.(10) for HDS of S_3 as Eq.(18), where k' is the global reaction rate constant for HYD pathway in HDS of S_3. Subsequently, to show the strength of nitrogen inhibition, ϕ is defined as a nitrogen inhibition factor as Eq.(19).

$$\phi = \frac{k'_{f,S_3} - k'}{k'_{f,S_3}} \tag{19}$$

As defined in Eq.(19), when the inhibition factor is larger, the reduction in the rate constant is enlarged implying a more potent nitrogen inhibition.

Combining kinetics of HDS and HDN with adsorption constants in

Table 5, we depict the evolution of the inhibition factor in Figure 10. It is shown, above 300°C, the nitrogen inhibition strength decays in the whole reaction coordinate and inflects in the middle since inhibition from N_1 lump dominates and drops with rate increase as demonstrated in Figure 9. By contrast, below 300°C, the nitrogen inhibition strength could be unexpectedly enhanced, rather than decrease. This appears to be counterintuitive since the nitrogen inhibition strength should have declined with the reducing amount of nitrogenous species removed by HDN. But it could be explained by our kinetic model(Eq.(10)). Since the dominant inhibitory

nitrogenous species is N_2 at relative low temperature and its concentration increases till a peak as shown in Figure 9, the nitrogen inhibition factor is then elevated by this increasing part.

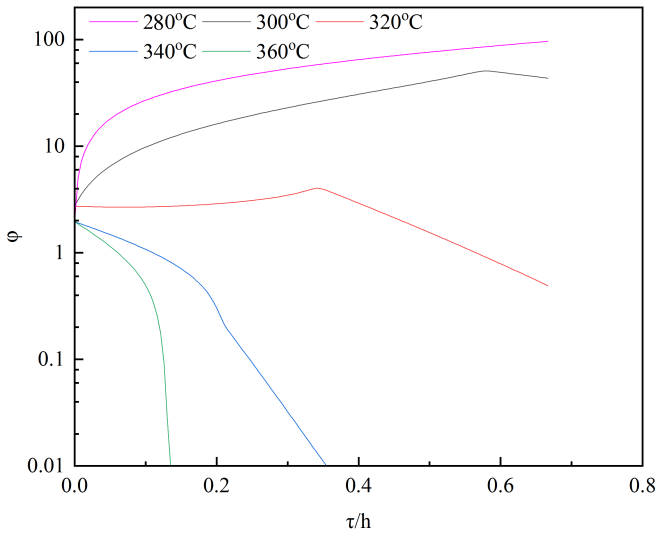

Figure 10.The profiles of the nitrogen inhibition factor under different temperatures(6.4MPa, 300 m^3_{STP}/m^3).

The explanation on the temperature dependency of nitrogen inhibition above is further corroborated by interaction between HDS of S_3 and HDN at 300°C. In Figure 11, nevertheless half of nitrogenous species is removed by HDN, HDS of S_3, which is dominantly inhibited by nitrogenous species, could remain an overall reaction order close to unity instead of being progressively faster and concaving down[12].

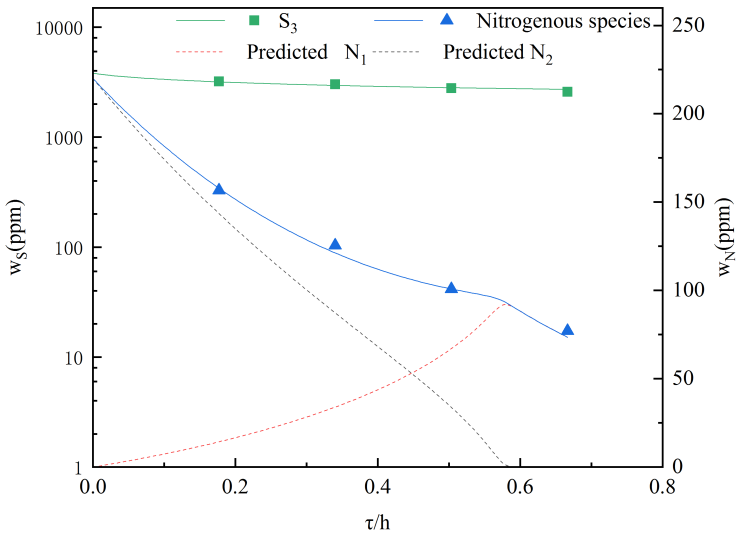

Figure 11.Interaction between HDS of S_3 and HDN of nitrogenous species(300°C,

6.4MPa, 300 m^3_{STP}/m^3).

8.3. Kinetic behaviors of sulfurous compounds

Combining the simulated results of all sulfur lumps together yields Figure 12, where four distinct stages can be identified.

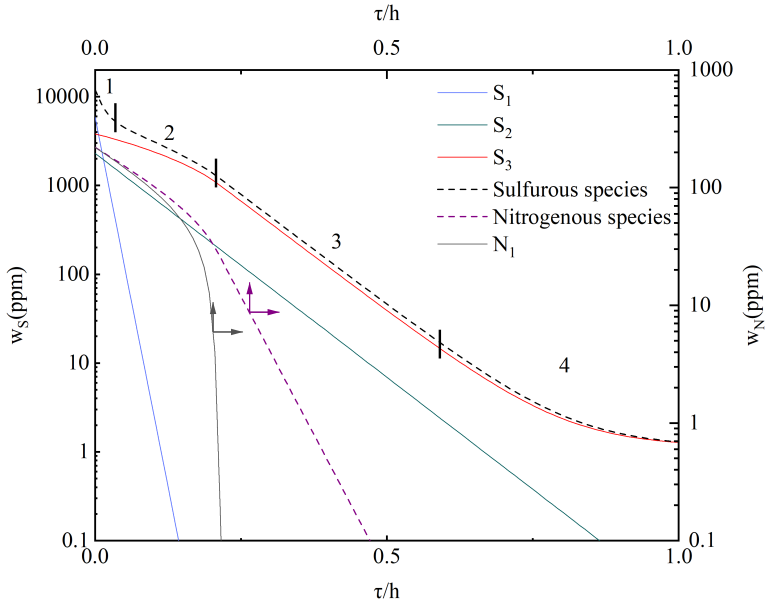

Figure 12. A quantitative picture of hydrodesulfurization.

In the stage 1, the HDS is fast and 60% of total sulfurous compounds is removed in short space time and the facile S_1 contributes the most via the predominant direct HDS. Simultaneously, HDN is going on, but due to strong self-inhibition effect, its rate is not high. When the S_1 is exhausted, the rate of HDS slows down and the stage 2 begins. The focus of the stage 2 shifts to HDN. Note that when N_1 lump is removed partly, the self-inhibition effect slumps and results in the acceleration of N_1 elimination to almost completion. Since the higher temperature causes the N_1 dominates the nitrogen inhibition effect as mentioned, with the complete removal of N_1, the nitrogen inhibition effect is also little afterwards. Consequently the HDS enters the stage 3 with the defining feature of its nitrogen-inhibition-free environment. Then the HDS speeds up and most of refractory S_2 and S_3 is removed via the hydrogenation pathway. However, the high rate of HDS cannot continue to the end. As explained in section 8.1, the thermodynamic

equilibrium of hydrogenation would take its toll here and bring the last UHDS stage. In this stage, the total sulfur consists of the most refractory S_3 and approach the equilibrium concentration in a decreasing rate. Besides, the kinetic behavior of total sulfur is approximate to the second order kinetics as proved by Ho et al.[40]. Despite the low order magnitude of the equilibrium concentration, it could be decisive in some cases like the high temperature and low pressure and cannot be ignored. It is noted that at higher temperatures(e.g. 380℃), the 4-stage model is still applicable with the disappearance of stage 2 due to the significant contribution of nitrogen-resistant DDS pathway to UHDS.

9. Conclusion

A three-lump kinetic model of UHDS is developed with simultaneous lumping kinetics of HDN and AHS by fully interpreted experimental data of diesel hydrotreating. By means of these models, we are able to get insights on thermodynamics, kinetics, and nitrogen inhibition in UHDS and conclude as follows.

Thermodynamic equilibrium is decisive in the selectivity and final result of UHDS at high temperature and low pressure, where the amount of sulfurous compounds stagnates at last to prohibit UHDS and DDS pathway of HDS for substituted dibenzothiophenic compounds becomes significant.

The nitrogen inhibition in our diesel feed is a tale of two lumps, the carbazole species (N_1) and its partially hydrogenated derivatives (N_2). Their adsorption capabilities vary with temperature dramatically, more N_1 are absorbed on active sites when temperature is above 300℃, and the opposite is true below 300℃. The strength of nitrogen inhibition to UHDS lowers down as reactions continue at above 300℃, but goes up even as the N_1 and N_2 are consumed in HDN at below 300℃.

Finally, in UHDS at relative low temperatures(e.g. <340℃), four distinct stages are identified as having markedly different conditions. In stage 1, the primary HDS reaction is the fast

hydrogenolysis of facile sulfurous compounds including benzothiophenes and thiophenes. As the rate of HDS reactions drops, stage 2 arrives. In this stage, nitrogenous species extremely inhibits HDS of the only remaining dibenzothiophenic compounds(DBTs) and thus the focus of reactions shifts from HDS to HDN. When nitrogenous species is gradually eliminated, hydrogenation pathway of refractory DBTs picks up the rate. Stage 2 ends when nitrogenous species is almost completely removed. At that time, the diesel feed enters stage 3 featured as nitrogen-free environment. In this environment, HDS of DBTs is in the highest rate and close to the first-order kinetics. However, the kinetic control would transform to thermodynamic control when hydrogenation of DBTs is close to the equilibrium, which is recognized as stage 4. In this stage, the concentration of most refractory DBTs lowers down asymptotically in a second-order fashion and hit a plateau decided by the thermodynamic equilibrium. At higher temperatures(e.g. 380℃), the stage 2 will disappear. This stage-wise model could help the development of trickle-bed reactors according to the characteristics of different stages.

10. Acknowledgement

We thank the National Key Research and Development Program of China (2017YFB0306600) and the financial support of China Petrochemical Corporation (Sinopec Group, 117006) for financial support.

11. Nomenclature

f:the mole fraction of vaporized diesel feed

L:the length of catalyst bed, m

$u_l = L \times LHSV$:the superficial liquid velocity, m/s

T: reaction temperature, K

R:the universal gas constant, J/mol·K

Subscript:

R:the reference conditions at 340℃

Superscript:

r: the backward reaction

j: the number of experiment

runs

p: the number of experiments in one run

P_{H_2}:the hydrogen pressure, MPa

C_i: the concentration of compound i, mol/m^3

τ : the space time, h

r_i:the reaction rate of i, mol/(m^3·s)

k_{f,N_i}: the reaction rate constant of the reaction for step i, $s^{-1}(MPa)^{-ni}$ at vaporized feed of f

K_i: the adsorption equilibrium constant for N_i in HDN reactions, m^3/mol

$(\Delta H_{ads})_i$:the adsorption enthalpy for N_i in active sites for HDN reactions, kJ/mol

k_{f,S_i}: the reaction rate constants for DDS of HDS for S_i lump at vaporized feed of f, $s^{-1}(MPa)^{-1}$

k'_{f,S_3}: the reaction rate constant for HYD of S_3 lump at vaporized feed of f, $s^{-1}(MPa)^{-0.5}$

E_i:the activation energy for reaction i, kJ/mol

K_{N_i}: the adsorption equilibrium constant for N_i in HDN reactions, m^3/mol

K_e: the equilibrium constant for S_3 lump in HDS reactions, m^3/mol

$(\Delta H_{ads})_{N_i}$: the adsorption enthalpy for N_i in HDS reactions, J/mol

k_{A_i}: the reaction rate constant for hydrogenation

reaction $i, J/mol$

SSE_i: the objective function for reaction i,mol/m^3

12. Literature Cited

1. Stanislaus A, Marafi A, Rana MS. Recent advances in the science and technology of ultra low sulfur diesel (ULSD) production. *Catal Today*. 2010;153(1-2):1-68. doi:10.1016/j.cattod.2010.05.011

2.Ho TC, Nguyen D. Modeling of competitive adsorption of nitrogen species in hydrodesulfurization. *Chem Eng Commun*. 2006;193(4):460-477. doi:10.1080/00986440500191669

3.Ho TC. Deep HDS of diesel fuel: Chemistry and catalysis. *Catal Today*. 2004;98(1-2 SPEC. ISS.):3-18. doi:10.1016/j.cattod.2004.07.048

4.Ho TC, Markley GE. Property-reactivity correlation for hydrodesulfurization of prehydrotreated distillates. *Appl Catal A Gen*. 2004;267(1-2):245-250. doi:10.1016/j.apcata.2004.03.009

5.Inoue S, Takatsuka T, Wada Y, Hirohama S, Ushida T. Distribution function model for deep desulfurization of diesel fuel. 2000;79:843-849.

6.Jarullah AT, Mujtaba IM, Wood AS. Kinetic parameter estimation and simulation of trickle-bed reactor for hydrodesulfurization of crude oil. *Chem Eng Sci*. 2011;66(5):859-871. doi:10.1016/j.ces.2010.11.016

7.Novaes L da R, de Resende NS, Salim VMM, Secchi AR. Modeling, simulation and kinetic parameter estimation for diesel hydrotreating. *Fuel*. 2017;209(April):184-193. doi:10.1016/j.fuel.2017.07.092

8.Chen Z, Feng S, Zhang L, et al. Molecular-level kinetic modelling of fluid catalytic cracking slurry oil hydrotreating. *Chem Eng Sci*. 2019:619-630. doi:10.1016/j.ces.2018.10.007

9. Albazzaz H, Marafi AM, Ma X, Ansari T. Hydrodesulfurization kinetics of middle distillates: A four-lumping model with consideration of nitrogen and aromatics inhibitions. *Energy and Fuels*. 2017;31(1):831-838. doi:10.1021/acs.energyfuels.6b02581
10. Yang H, Chen J, Briker Y, Szynkarczuk R, Ring Z. Effect of nitrogen removal from light cycle oil on the hydrodesulphurization of dibenzothiophene, 4-methyldibenzothiophene and 4,6-dimethyldibenzothiophene. *Catal Today*. 2005;109(1-4):16-23. doi:10.1016/j.cattod.2005.08.028
11. Chen J, Yang H, Ring Z. HDS kinetics study of dibenzothiophenic compounds in LCO. *Catal Today*. 2004;98(1-2 SPEC. ISS.):227-233. doi:10.1016/j.cattod.2004.07.036
12. Ho TC. Inhibiting effects in hydrodesulfurization of 4,6-diethyldibenzothiophene. *J Catal*. 2003;219(2):442-451. doi:10.1016/S0021-9517(03)00215-X
13. Furimsky E, Massoth FE. Hydrodenitrogenation of petroleum. *Catal Rev - Sci Eng*. 2005;47(3):297-489. doi:10.1081/CR-200057492
14. Prins R, Jian M, Flechsenhar M. Mechanism and kinetics of hydrodenitrogenation. *Polyhedron*. 1997;16(18):3235-3246. doi:10.1016/S0277-5387(97)00111-3
15. Nagai M, Sawahiraki K, Kabe T. Hydrodenitrogenation of Carbazole on MoO3-AI2O3 Catalyst? *Nippon Kagaku Kaishi*. 1980;1980(1):69-73. doi:10.1246/nikkashi.1980.69
16. Laredo GC, Montesinos A, De Los Reyes JA. Inhibition effects observed between dibenzothiophene and carbazole during the hydrotreating process. *Appl Catal A Gen*. 2004;265(2):171-183. doi:10.1016/j.apcata.2004.01.013
17. Laredo GC, Altamirano E, De los Reyes JA. Inhibition effects of nitrogen compounds on the hydrodesulfurization of dibenzothiophene: Part 2. *Appl Catal A Gen*. 2003;243(2):207-214. doi:10.1016/S0926-860X(02)00321-6
18. Ho TC, Qiao L. Competitive adsorption of nitrogen species in HDS: Kinetic characterization of hydrogenation and hydrogenolysis sites. *J Catal*. 2010;269(2):291-301.

doi:10.1016/j.jcat.2009.11.012

19. Bandyopadhyay R, Upadhyayula S. Thermodynamic analysis of diesel hydrotreating reactions. *Fuel*. 2018;214(February):314-321. doi:10.1016/j.fuel.2017.10.015

20. Wu G, Yin Y, Chen W, et al. Catalytic kinetics for ultra-deep hydrodesulfurization of diesel. *Chem Eng Sci*. 2020;214:115446.

21. Yongtan Yang; Zheng Wang. Determination and Distribution of Sulfur Compounds in Coked Gasoline by Gas Chromatography-Sulfur Chemiluminescence Detection.

22. Yang Y. Distribution determination of nitrogen compounds in catalytic diesel oil using gas chromatography. *Chinese J Chromatogr (Se Pu)*. 2008;26(4):478-483. doi:10.1016/s1872-2059(08)60023-1

23. Guang-tong Xu, Ze-long Liu, Yu-rui Yang, Shi-kong Shen WL. Determination of diesel fuel composition by near infrared spectroscopy and its application. *ACTA Pet Sin*. 2002;18(4):65-71.

24. Chowdhury R, Pedernera E, Reimert R. Trickle-bed reactor model for desulfurization and dearomatization of diesel. *AIChE J*. 2002;48(1):126-135. doi:10.1002/aic.690480113

25. Chen J, Wang N, Mederos F, Ancheyta J. Vapor-liquid equilibrium study in trickle-bed reactors. *Ind Eng Chem Res*. 2009;48(3):1096-1106. doi:10.1021/ie8006006

26. Chen J, Mulgundmath V, Wang N. Accounting for Vapor - Liquid Equilibrium in the Modeling and Simulation of a Commercial Hydrotreating Reactor. *Ind Eng Chem Res*. 2011:1571-1579.

27. Chávez LM, Alonso F, Ancheyta J. Vapor-liquid equilibrium of hydrogen-hydrocarbon systems and its effects on hydroprocessing reactors. *Fuel*. 2014;138:156-175. doi:10.1016/j.fuel.2014.03.062

28. Miller JT, Hineman MF. Non-first-order hydrodenitrogenation kinetics of quinoline. *J Catal*. 1984;85(1):117-126. doi:10.1016/0021-9517(84)90115-5

29.Sarbak Z. Catalytic hydrodenitrogenation of carbazole and some of its partially hydrogenated intermediate products. *React Kinet Catal Lett*. 1986;32(2):449-455. doi:10.1007/BF02068350

30.Devocht BR, Thybaut JW, Kageyama N, Toch K, Oyama ST, Marin GB. Balance between model detail and experimental information in steam methane reforming over a Ni/MgO-SiO 2 catalyst. *AIChE J*. 2019;65(4):1222-1233. doi:10.1002/aic.16512

31.Nagai M, Goto Y, Miyata A, et al. Temperature-programmed reduction and XRD studies of ammonia-treated molybdenum oxide and its activity for carbazole hydrodenitrogenation. *J Catal*. 1999;182(2):292-301. doi:10.1006/jcat.1998.2365

32.Ma X, Sakanishi K, Mochida I. Hydrodesulfurization Reactivities of Various Sulfur Compounds in Diesel Fuel. *Ind Eng Chem Res*. 1994;33(2):218-222. doi:10.1021/ie00026a007

33.Ho TC. A theory of ultradeep hydrodesulfurization of diesel in stacked-bed reactors. *AIChE J*. 2018;64(2):595-605. doi:10.1002/aic.15969

34.Kwak C, Jung Joon Lee, Jun Sang Bae, Sang Heup Moon. Poisoning effect of nitrogen compounds on the performance of CoMoS/Al2O3catalyst in the hydrodesulfurization of dibenzothiophene, 4-methyldibenzothiophene, and 4,6-dimethyldibenzothiophene. *Appl Catal B Environ*. 2001;35(1):59-68. doi:10.1016/S0926-3373(01)00233-8

35.Egorova M, Prins R. Hydrodesulfurization of dibenzothiophene and 4,6-dimethyldibenzothiophene over sulfided NiMo/γ-Al2O3, CoMo/γ-Al 2O3, and Mo/γ-Al2O3 catalysts. *J Catal*. 2004;225(2):417-427. doi:10.1016/j.jcat.2004.05.002

36.Farag H, Whitehurst DD, Sakanishi K, Mochida I. Carbon versus alumina as a support for Co-Mo catalysts reactivity towards HDS of dibenzothiophenes and diesel fuel. *Catal Today*. 1999;50(1):9-17. doi:10.1016/S0920-5861(98)00476-3

37.Thomas E. and RPDD. Technical Data Book –Petroleum Refining. 1997:pp.217.

38. Sakanishi K, Nagamatsu T, Mochida I, Whitehurst DD. Hydrodesulfurization kinetics and mechanism of 4,6- dimethyldibenzothiophene over NiMo catalyst supported on carbon. *J Mol Catal A Chem*. 2000;155(1-2):101-109. doi:10.1016/S1381-1169(99)00323-4

39. Rana MS, Al-Barood A, Brouresli R, Al-Hendi AW, Mustafa N. Effect of organic nitrogen compounds on deep hydrodesulfurization of middle distillate. *Fuel Process Technol*. 2018;177(April):170-178. doi:10.1016/j.fuproc.2018.04.014

40. Ho TC, Aris R. On apparent second-order kinetics. *AIChE J*. 1987;33(6):1050-1051. doi:10.1002/aic.690330621

41. Korsten H, Hoffmann U. Three-Phase Reactor Model for Hydrotreating in Pilot Trickle-Bed Reactors. *AIChE J*. 1996;42(5):1350-1360. doi:10.1002/aic.690420515